# Remote Photothermal Actuation of Underwater Bubble toward Arbitrary Direction on Planar Slippery Fe$_3$O$_4$-Doped Surfaces

*Chao Chen, Zhouchen Huang, Lu-An Shi, Yunlong Jiao, Suwan Zhu, Jiawen Li, Yanlei Hu,\* Jiaru Chu, Dong Wu,\* and Lei Jiang*

Unidirectional underwater gas bubble (UGB) transport on a surface is realized by buoyant force or wettability gradient force ($F_{wet-grad}$) derived from a tailored geography. Unfortunately, intentional control of the UGB over transport speed, direction, and routes on horizontal planar surfaces is rarely explored. Herein reported is a light-responsive slippery lubricant-infused porous surface (SLIPS) composed of selective lubricants and super-hydrophobic micropillar-arrayed Fe$_3$O$_4$/polydimethylsiloxane film. Upon this SLIPS, the UGB can be horizontally actuated along arbitrary directions by remotely loading/discharging unilateral near-infrared (NIR) stimuli. The underlying mechanism is that $F_{wet-grad}$ can be generated within 1 s in the presence of a NIR-trigger due to the photothermal effect of Fe$_3$O$_4$. Once the NIR-stimuli are discharged, $F_{wet-grad}$ vanishes to break the UGB on the SLIPS. Moreover, performed are systematic parameter studies to investigate the influence of bubble volume, lubricant rheology, and $F_{wet-grad}$ on the UGB steering performance. Fundamental physics renders the achievement of antibuoyancy manipulation of the UGBs on an inclined SLIPS. Significantly, steering UGBs by horizontal SLIPS to configurate diverse patterns, as well as facilitating light-control-light optical shutter, is deployed. Compared with the previous slippery surfaces, light-responsive SLIPS is more competent for manipulating UGBs with controllable transport speed, direction, and routes independent of buoyancy or geography derivative force.

## 1. Introduction

Achieving the controllable manipulation of gas bubbles in aqueous media is of great importance for both academic investigations and industrial explorations because of its potential applications in wastewater treatment,[1,2] recovery of valuable minerals from ores,[3] pressure sensors,[4] transportation pipe remediation from erosions,[5–8] gas-evolving electrochemistry,[9,10] areolation, and ozone treatment.[11–14] Thus, ceaseless efforts has been paved for realizing this target by virtue of designing plenty of tailored geography and biomimetic surfaces. For instance, inspired by natural species of cactus spine, Yu et al. reported a hydrophobic copper cone composed of low-surface-tension coatings and conical geography, which was utilized for transporting bubbles in the direction of both buoyancy and antibuoyancy due to the giant Laplace pressure difference at bilateral.[15] Jiang and his coworkers developed a rotating super-hydrophobic helix by chemical etching and hydrophobic fume nanoparticle (NP) modification, which was successfully applied for controllable and directional underwater bubble transport.[16] Zhang et al. prepared diverse super-hydrophobic poly(methyl methacrylate) (PMMA) sheets such as five-pointed star, triangle, circular, and ellipse by grafting silica NPs and a subsequent CO$_2$-laser cutting method for manipulating underwater gas bubbles.[17] Obviously, these methods should be summarized as one typical category that has similarities of driving force named as wettability gradient force originating from platform's geography.

Dr. C. Chen, Z. Huang, Dr. Y. Jiao, Dr. S. Zhu, Prof. J. Li, Prof. Y. Hu, Prof. J. Chu, Prof. D. Wu
Hefei National Laboratory for Physical Sciences at the Microscale
Key Laboratory of Precision Scientific Instrumentation of Anhui Higher Education Institutes
CAS Key Laboratory of Mechanical Behavior and Design of Materials
Department of Precision Machinery and Precision Instrumentation
University of Science and Technology of China
Hefei 230026, China
E-mail: huyl@ustc.edu.cn; dongwu@ustc.edu.cn

L.-A. Shi
Division of Nanomaterials and Chemistry
Hefei National Laboratory for Physical Sciences at the Microscale
Collaborative Innovation Center of Suzhou Nano Science and Technology
CAS Center for Excellence in Nanoscience
Hefei Science Center of CAS
Department of Chemistry
University of Science and Technology of China
Hefei 230026, China

Prof. L. Jiang
Key Laboratory of Bio-inspired Materials and Interfacial Science
Technical Institute of Physics and Chemistry
Chinese Academy of Sciences
Beijing 100190, China

Another emerging category developed by researchers should be assigned to pitcher-plant-inspired slippery lubricant-infused porous surface (SLIPS) that exhibit excellent ability of manipulating gas bubbles dependent on buoyancy. For example, Zhang et al. fabricated morphology-gradient slippery PMMA sheets by $CO_2$-laser cutting, super-hydrophobic modification, and fluorinert infusion, which was demonstrated a favorable platform applicable to the directional and continuous bubble delivery in aqueous environment.[18] Yu et al. presented a lubricant-infused slippery surface constructed by filter paper, polydimethylsiloxane (PDMS), hydrofluorosilicic acid, and silicone oil with outstanding water repellency, which was shaped for in situ capture and delivery of bubbles in aqueous environment.[19] Jiao et al. designed a lubricated slippery surface fabricated by femtosecond laser for buoyancy-driven bubble self-transport and gas capture.[20] More recently, Guo et al. achieved the dynamic control between pinning and sliding for liquid droplet and bubble on an amphibious slippery Fe/PDMS gel surface by loading/discharging external magnetic stimuli.[21] In brief, the previous investigations have greatly advanced the physical basis and practical techniques with respect to manipulating gas bubbles in aqueous media.

However, several severe blockages arise subsequently: 1) Most of the hydrophobic/aerophilic platforms were fabricated by chemical etching or hydrophobic NP modification, which is not eco-friendly and time-consuming.[15–20] 2) Achieving bubble directional transport and delivery is either limited to wettability gradient force arising from platform's geometry (e.g., tapered shapes) or dependent on buoyant force, which hindered its practical application in dynamic underwater gas bubble (UGB) control (e.g., pinning and sliding) on horizontal substrates.[15–20] Though controllable motion between pinning and sliding for UGB has been realized by a magnetic stimulus, the driving force is dominated by buoyant force, and thus can only drive the bubble at tilted surface.[21] 3) To the best of our knowledge, previous explorations are only functional at realizing unidirectional UGB transport, whereas the controllable moving speed, direction, and routes for UGB on horizontal platform have been rarely demonstrated. In this regard, seeking a more facile, eco-friendly, and morphology/buoyancy-independent smart surface for steering UGBs toward arbitrary directions at the horizontal surface is still a timely challenge and is an urgent need.

In this work, we report a light-responsive SLIPS composed of silicone oil and super-hydrophobic micropillar-arrayed $Fe_3O_4$/PDMS film (PAF) that is fabricated by one-step femtosecond laser vertically crossed scanning. Based on this intelligent film, a new strategy for horizontally actuating bubble toward arbitrary directions is proposed by simply loading/discharging unilateral near-infrared (NIR)-stimuli. The underlying mechanism is that a giant wettability gradient force ($F_{wet-grad}$) induced by temperature difference would be generated within 1 s in the presence of a unilateral NIR-trigger due to the photothermal effect of $Fe_3O_4$ embedded in SLIPS. Once the NIR-stimuli are discharged, the instantaneous vanish of $F_{wet-grad}$ would break UGB on the horizontal SLIPS from sliding to pinning. Moreover, we quantitatively study the influence of bubble volume, $F_{wet-grad}$ and sliding velocity on the underwater bubble steering performance. In addition, the effect of lubricant rheological properties (surface tensions and viscosities) on the bubble hydrokinetics is systematically investigated. Fundamental physics renders us the achievement of antibuoyancy manipulating various UGBs with ease on inclined substrate. Significantly, on-demand steering the UGBs on horizontal SLIPS to configure diverse patterns and regulate optical shutter is deployed. Compared with the previously reported Nepenthes-inspired slippery surfaces, this versatile light-triggered SLIPS independent of geography/buoyancy is more functional at precisely manipulating UGB transport with controllable moving speed, direction, and routes. This study will provide an inspiration for researchers to design smart slippery surfaces for the controllable manipulation of gas bubbles and further bloom the studies of gas bubbles in aqueous mediums.

## 2. Results and Discussion

### 2.1. Facile Fabrication of Light-Triggered SLIPS for Steering UGBs at Arbitrary Direction

Strategy for the fabrication of smart SLIPS is composed of five crucial steps (**Figure 1**a). First, the photothermal material of $Fe_3O_4$ NPs was uniformly mixed with the PDMS gel by vigorous stirring overnight (Figure S3, Supporting Information). Subsequently, their mixture should be carefully casted into a home-made groove and allowed self-leveling and bubble-removing for 30 min in the vacuum oven. Thereafter, a flexible $Fe_3O_4$ NPs/PDMS film could be harvested after an annealing process at 80 °C for 2 h. Furthermore, a super-hydrophobic PAF with water contact angle of 150.3 ± 1.5° could be facilely manufactured by one-step laser vertically scanning which has been adopted as an emerging technique to modify the wettability of various materials due to its advantages of high-efficiency, low heat-effect, and good controllability, where the length and height of pillars and their intervals are characterized as 57.7, 83.3, and 38.5 μm (Figure 1b,c and Figure S4, Supporting Information), respectively. It is noteworthy that the components in PAF maintained their original lattice plane after laser ablation because femtosecond laser has a considerable advantage of small heat-effect, which had been verified by X-ray diffraction spectrums (Figure S1, Supporting Information).[22] Finally, by virtue of the capillary effect, low-surface-tension silicone oil with a typical viscosity of 10 mPa s was carefully infused into the as-prepared PAF to fabricate the desirable SLIPS (detailed procedure can be seen in the Experimental Section). Considering that the thickness of lubricant layer is indeed relevant with the height of $Fe_3O_4$/PDMS pillars, which has been roughly estimated as 83.3 ± 5 μm in the current system. Based on this planar SLIPS, we could horizontally steer UGB toward arbitrary directions by regulating the irradiation sites of NIR (Figure 1d and Movie S1, Supporting Information). Moreover, the durability test had been also conducted using this light-triggered SLIPS and the results demonstrate that the current multi-phase system can slide UGB for at least 60 cycles without interrupting its velocity and direction (Figure S5, Movie S7, Supporting Information). UGB on smart SLIPS should present a stationary state at the absence
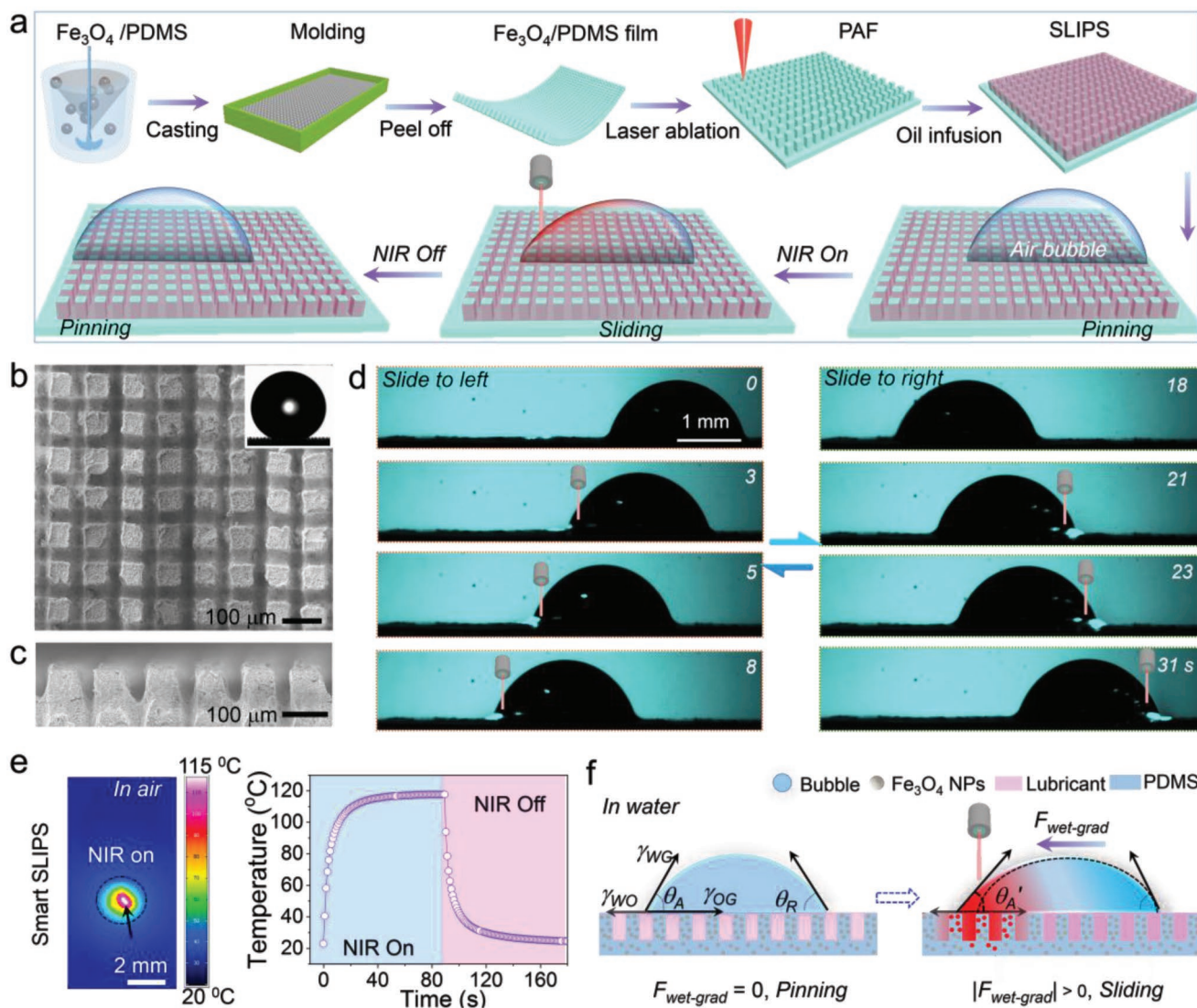
**Figure 1.** Fabrication of smart SLIPS and its characterizations. a) Schematic diagram illustrating the fabricating strategy of SLIPS by successive blending, molding, laser scanning, oil infusion processes. The bubble manipulation strategy by loading/discharging NIR-actuation is illustrated in the lower row. SEM images of b) top view and c) sectional view for the resultant PAF; the inset represents the water contact angle of as-prepared PAF. d) The captured clips for NIR-actuating UGB on SLIPS (lubricant: silicone oil, 10 mPa s) to demonstrate its controllable sliding directions by tuning the NIR irradiation sites. e) NIR image and its corresponding temperature versus time curve for NIR-stimuli (power density: $1.1 \times 10^2$ mW cm$^{-2}$, altitude: 8 cm) applied on SLIPS in air. f) The underlying mechanism for NIR-actuating UGB by smart SLIPS.

of NIR due to the identical values for advancing angle ($\theta_A$) and receding angle ($\theta_R$), which signified that the UGB was at force balance according to a classical wettability gradient force ($F_{\text{wet-grad}}$) formula[14]

$$F_{\text{wet-grad}} = \gamma \times R_B \times (\cos\theta_A - \cos\theta_R) \tag{1}$$

where $\gamma$ is the surface tension of water ($7.2 \times 10^{-2}$ N m$^{-1}$) and $R_B$ represents the character length of UGB on SLIPS. Once NIR was deployed, the local temperature for SLIPS increased from 22 to 41 °C within 1 s (Figure 1e). Hence, the decrease of $\theta_A$ would initiate an asymmetric Laplace force, which was indeed induced by the decreased surface tension of lubricant ($\gamma_{OG}$) with the elevated local temperature derived from

photothermal effect in Fe$_3$O$_4$ NPs (Figure 1f and detailed discussion can be seen in Figure S2, Supporting Information).[23] In consequence, the switchable pinning/sliding for UGB SLIPS at arbitrary direction could be readily realized by taking advantage of loading/discharging selectively unilateral NIR-stimuli, which was essentially dominated by the presence/absence of $F_{\text{wet-grad}}$.

## 2.2. NIR-Actuating UGBs with Different Size on Horizontal SLIPS

In practical implementation, a versatile SLIPS for manipulating bubbles with different size is highly desirable, so the
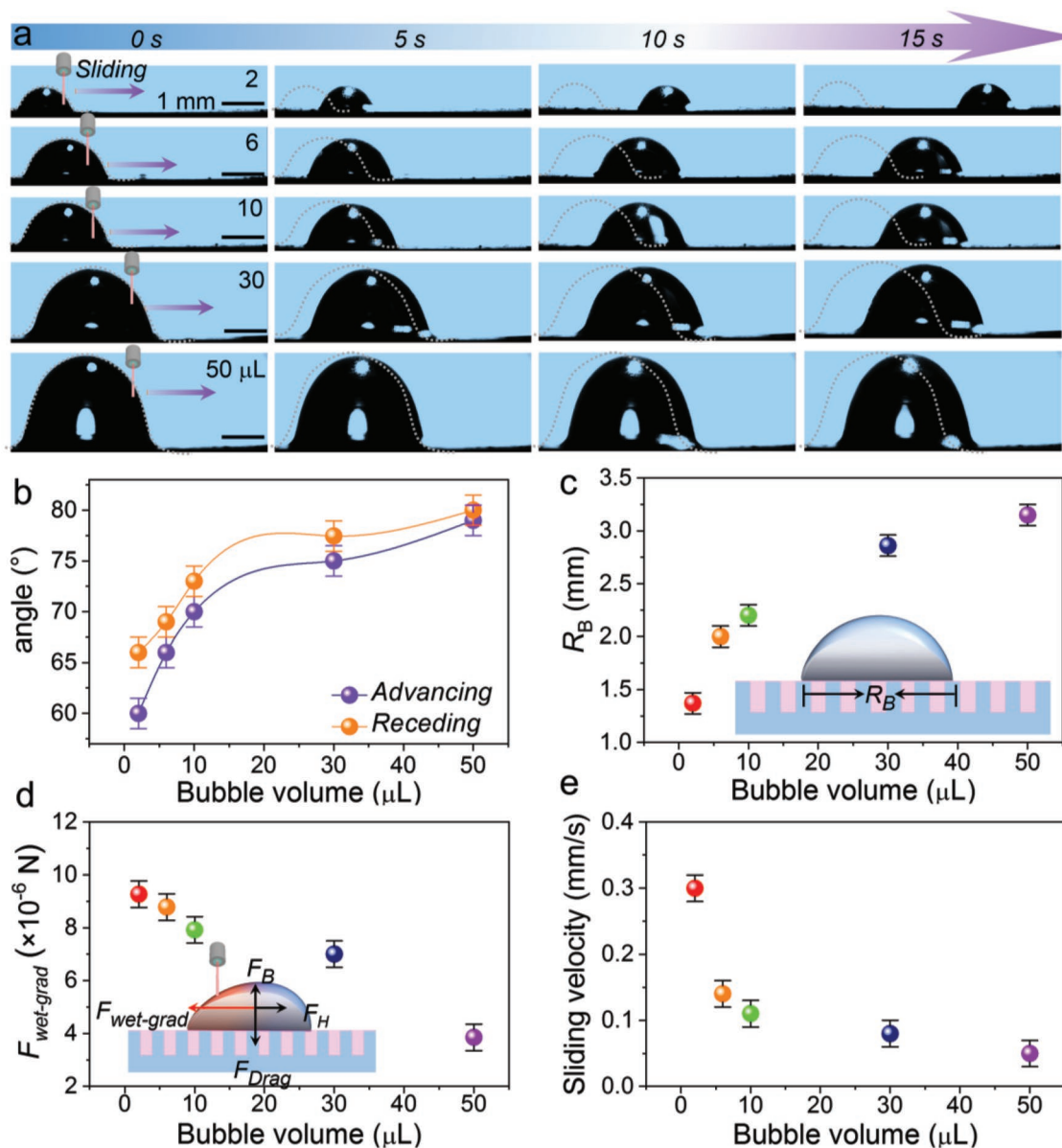
**Figure 2.** Hydrokinetics analysis for NIR-actuating UGBs with different size on horizontal SLIPS. a) The captured optical images for NIR-actuating (power density: $1.1 \times 10^2$ mW cm$^{-2}$, altitude: 8 cm) UGBs with volumes of 2, 6, 10, 30, and 50 µL on smart SLIPS (lubricant: silicone oil, 10 mPa s), respectively. The variations of b) advancing and receding angles, c) local length, d) wettability gradient force, and e) sliding velocity as a function of bubble volume for diverse UGBs on smart SLIPS.

smart SLIPS is expected to be extensively adaptive for steering UGBs with various volumes. Accordingly, the underwater hydrokinetics for air bubbles with volume of 2, 6, 10, 30, and 50 µL exposed to a tracing NIR-stimuli had been in situ monitored by a computer-connected charge-coupled device (**Figure 2**a and Movie S2, Supporting Information). The moving UGB actuated by NIR-stimuli on the planar SLIPS should be subjected to four acting forces in the horizontal and perpendicular directions, which could be categorized as the forward driving force $F_{\text{wet-grad}}$, backward hydrodynamic resistance ($F_H$), upward buoyant force ($F_B$), and downward drag force of lubricant preventing the gas bubble from disorbition ($F_{\text{Drag}}$). Wherein, $F_H$, as a combination of lubricant

and liquid media's viscous forces, is opposite to the sliding direction of UGB on SLIPS.[24] Its value could be described as follows[25]

$$F_H \approx \alpha\left(\mu_o + \mu_l\right)v\pi R \tag{2}$$

where $\alpha$ is a numerical factor, $\mu_o$ is the viscosity of lubricant oil, $\mu_l$ is the viscosity of liquid media, and $v$ is the droplet velocity. Accordingly, $F_H$ would increase with increasing bubble sliding velocity. By combining Equations (1) and (2), we can roughly infer that at the initial stage of NIR-actuating motion of the UGB, $F_{\text{wet-grad}} > F_H$, the UGB on SLIPS would accelerate until $F_{\text{wet-grad}} > F_H$, when the UGB moves with

a constant velocity. The UGB would stop when $F_{\text{wet-grad}} = 0$ without NIR action.

Hereby, the UGBs with different volumes had disparate buoyant force, which resulted in the apparently distinctive wettability on smart SLIPS. The contact angles for five UGBs (UGBCA) on horizontal planar SLIPS were measured as 66°, 69°, 73°, 77°, and 80°, respectively. After the unilateral NIR-stimuli was applied on five disparate UGBs on smart SLIPS, $\theta_A/\theta_R$ and $R_B$ were changed to 60/66°, 66/69°, 70/73°, 75/77°, 79/80° and 1.37, 2.01, 2.20, 2.86, 3.15 mm (Figure 2b,c), respectively. The larger the bubble volume, the larger the bubble local diameter as well as $\theta_A/\theta_R$. According to Equation (1), the corresponding $F_{\text{wet-grad}}$ originated from the asymmetric wettability for five disparate UGBs were quantitatively calculated as 9.27, 8.78, 7.92, 7.00, and 3.86 ($\times 10^{-6}$) N (Figure 2d), respectively. That is, the bigger the bubble size, the larger the bubble $F_{\text{wet-grad}}$. In addition, the consumed time for five disparate UGBs sliding an identical distance of 6 mm was recorded as 18, 26, 35, 37, and 120 s (Movie S1, Supporting information), respectively. Thereby, the average sliding velocities for five disparate UGBs were calculated as 30, 14, 11, 8, and 5 ($\times 10^{-2}$) mm s$^{-1}$ (Figure 2e), respectively. Based on the quantification of the forces acting during the transport process, the larger the bubble volume, the smaller the bubble driving force $F_{\text{wet-grad}}$. As a result, the mechanism of decrease in transport velocity upon increasing the underwater gas bubble volume should be attributed to the decrease of a dominant driving force of $F_{\text{wet-grad}}$. The driving force ($F_{\text{wet-grad}}$) and sliding velocity ($v$) for UGB on horizontal SLIPS had been demonstrated inversely proportional to the bubble size, which revealed that this smart system composed of SLIPS and NIR-stimuli was more sensitive and effective for steering small gas bubbles in aqueous media.

## 2.3. NIR-Actuating UGBs on Horizontal SLIPS with Different Lubricant Species

The dynamic behavior for UGB on smart SLIPS was dominated by the numerical values of $R_B$, $\theta_A$, $\theta_R$, and $F_{\text{Drag}}$ that were highly dependent on the lubricant species with different surface tensions ($\gamma_{\text{OG}}$) and viscosities ($\eta$). To investigate the effect of lubricant rheology properties on the UGB sliding velocity, we had successively fabricated five disparate SLIPSs via the infusion of FC3283 (perfluoro-tri-n-propylamine), silicone oil, liquid paraffin, hexadecane, and castor oil into five as-prepared PAFs. Wherein, the corresponding surface tensions and viscosities were obtained as 1.60/2.06/2.72/3.40/4.44 ($\times 10^{-2}$) N m$^{-1}$ and 0.82/10/230/0.72/600 mPa s, respectively. Accordingly, the dynamic behaviors for NIR-actuating UGBs (10 µL) on five disparate SLIPSs could be observed in **Figure 3**a (Movie S3, Supporting Information). The BCA ($\theta_G$) on five smart SLIPSs exhibited an elevating tendency with the increase of lubricant surface tensions, whereas the local length of UGBs was inclined to decrease. Furthermore, the values of $\theta_A$ and $\theta_R$ for NIR-actuating UGBs on five smart SLIPSs with different lubricant species were successively characterized as 52°, 63°, 71°, 78°, 100° and 63°, 67°, 75°, 82°, 102° (Figure 3b), respectively. Accordingly, their corresponding cosine values had been

calculated as 0.615, 0.453, 0.325, 0.207, −0.173 and 0.453, 0.39, 0.258, 0.139, −0.207, respectively. Notably, the local length ($R_B$) for UGBs on five smart SLIPSs was inversely proportional to the surface tensions of lubricant oils and the relative measurements for $R_B$ were recorded as 2.1, 2.0, 1.8, 1.7, and 1.3 mm (Figure 3c), respectively. As a result, the values of $F_{\text{wet-grad}}$ for NIR-actuating UGBs on five planar SLIPSs could be calculated as 24.5, 9.0, 8.7, 8.5, and 3.3 ($\times 10^{-6}$) N (Figure 3d), respectively. The smaller the lubricant surface tension, the larger the bubble driven force. Nevertheless, the recorded sliding velocities for UGBs on five smart SLIPSs were dramatically independent on the surface tension of lubricants but proportional to the lubricant viscosity, which implied the kinetics for NIR-actuating UGBs could be easily controlled by tuning the lubricant species (Figure 3e). The mechanism could be revealed according to Equation (2), which unfolds that the larger the lubricant viscosity, the larger the bubble sliding resistance $F_H$. As a result, the lubricant viscosity can determine the bubble sliding velocity through decreasing and elevating hydrodynamic resistance.

## 2.4. Antibuoyancy Steering UGB on Inclined SLIPS

In addition to a horizontal SLIPS, achieving the controllable dynamics for UGBs on an inclined SLIPS is of great significance for extensively adaptive applications. In this regard, NIR-actuating UGBs should be capable of moving against buoyancy even though the smart SLIPS has been settled at an oblique terrain. For clarity, the UGB on an inclined SLIPS should be subjected to the uphill component force of buoyancy ($F_{B//}$), downhill resistance arising from contact angle hysteresis ($F_{\text{CAH}}$), and $F_H$, component force perpendicular to the inclined SLIPS ($F_B\perp$) and $F_{\text{Drag}}$, where $F_{B//}$ is considered as the dominant force actuating the targeted UGB sliding uphill at the absence of NIR-stimuli (**Figure 4**a). Once the unilateral NIR was applied, the light-induced downhill $F_{\text{wet-grad}}$ at the initial stage is larger than the integration of $F_{B//}$ and $F_H$ and will drag UGB moving against buoyancy. Until $F_{\text{wet-grad}} = F_{B//} + F_H$, the UGB would slide in a constant speed. On this basis, the UGB on inclined SLIPS could be readily steered on-demand to slide uphill/downhill by discharging/loading NIR-stimuli.

Accordingly, the dynamic control for a typical UGB (10 µL) on smart SLIPS (inclined angle ≈ 6°) had been conducted by loading/discharging NIR-stimuli (Figure 4b and Movie S4, Supporting information). Under the assistance of buoyancy, the UGB tended to slide upward along smart SLIPS at a constant velocity of 0.1 mm s$^{-1}$, whereas it was immediately stopped and then steered downhill at a constant speed of 0.025 mm s$^{-1}$ by loading unilateral NIR-stimuli (Figure 4c). Therein, the experimental measurements and theoretical calculations had been successfully implemented to clarify this controllable hydrokinetics. When NIR was loaded, the corresponding $\theta_A$ had decreased from 70° to 66°, whereas $\theta_R$ tended to be stabilized at 72° (Figure 4d). Additionally, $R_B$ could be slightly tuned between 2.2 and 2.0 mm by loading/discharging NIR-stimuli. According to Equation (1), the calculated |$F_{\text{wet-grad}}$| for UGB on inclined SLIPS could be readily switchable between 11.4 and
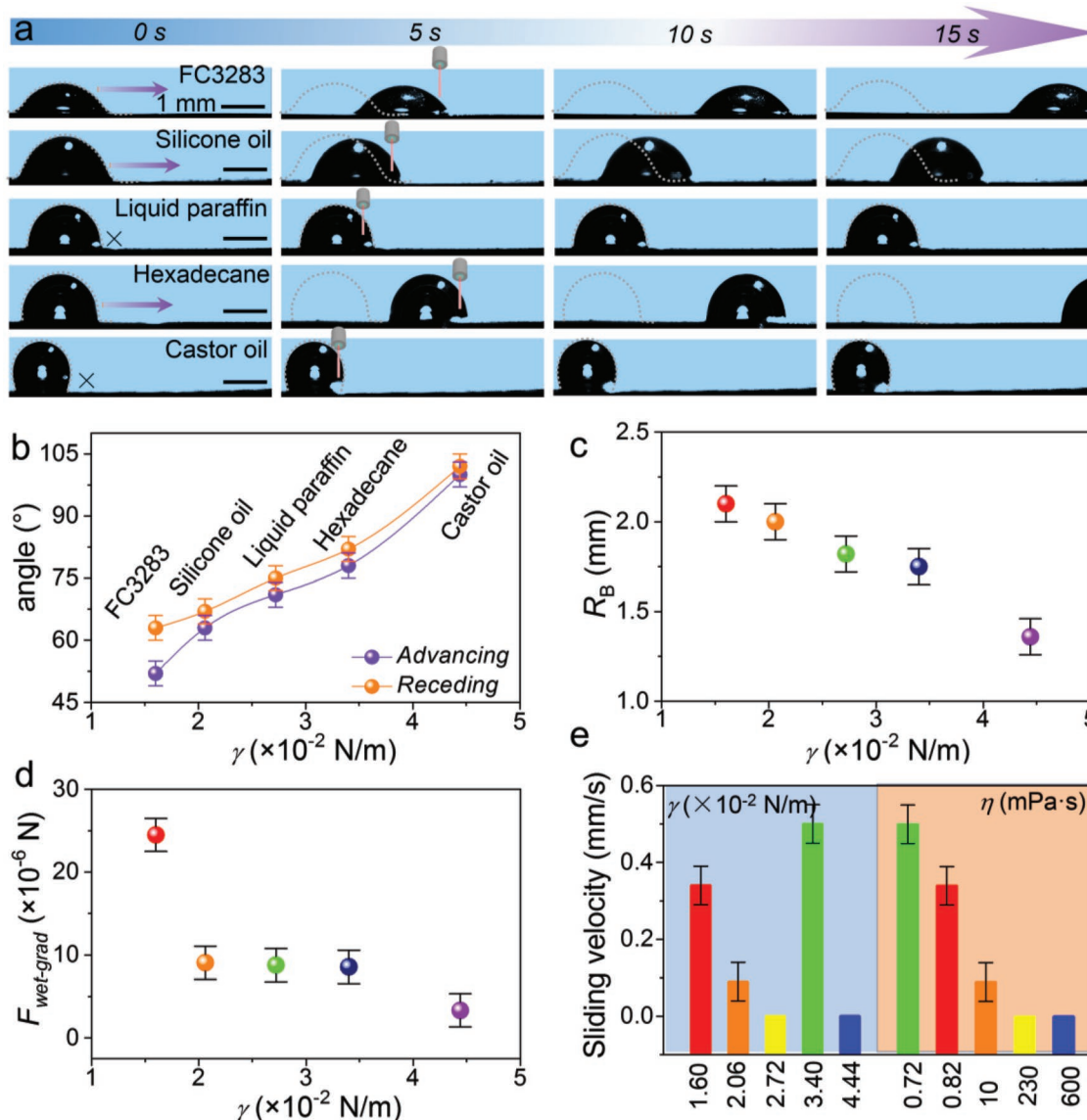
**Figure 3.** Effect of lubricant rheology on UGB steering performance. a) The captured optical images for NIR-actuating (power density: $1.1 \times 10^2$ mW cm$^{-2}$, altitude: 8 cm) UGB (10 µL) on smart SLIPSs infused with FC3283, silicone oil, liquid paraffin, hexadecane, and castor oil, respectively. The change of b) advancing and receding angles, c) local length, and d) wettability gradient force versus lubricant surface tensions for typical UGBs (10 µL) on SLIPS. e) Comparisons for bubble sliding velocity under various surface tensions/viscosities.

4.3 ($\times 10^{-6}$) N by loading/unloading NIR (Figure 4e). In regard of buoyant force as a constant of $10^{-5}$ N, so the driving force for UGB (10 µL) on inclined SLIPS was controllable between $-1.4$ and 5.7 ($\times 10^{-6}$) N by loading/unloading NIR (Figure 4f). It is noteworthy that the relative ratio for theoretical driving forces acting on UGB during the uphill/downhill processes ($F_{upill}/F_{downhill} = 5.7/1.4$) is very consistent with the measured sliding velocity relationship ($v_{upill}/v_{downhill} = 0.10/0.025$), which verified that the fabricated physical model is highly reliable.

Considering that $F_{B//}$ is a component force dependent of bubble volume ($V_B$) and inclined angle ($\alpha$), which can be written as

$$F_{B//} = \rho g V_B \sin \alpha \tag{3}$$

So we could further obtain an empirical Equation (4) for evaluating the critical angles ($\alpha_{cri}$) for antibuoyancy steering UGBs on an inclined SLIPS by combining Equations (1) and (3)

$$\sin \alpha = \frac{\gamma \times R_B \times (\cos \theta_A - \cos \theta_R)}{\rho g V_B} \tag{4}$$

The method for verifying $\alpha_{cri}$ is divided into three crucial processes including i) buoyancy-driven UGB sliding uphill with a constant velocity ($v$) without NIR-stimuli, ii) NIR-actuating UGB decelerated with a constant acceleration ($a$), and iii) NIR-actuating UGB pinning on the inclined SLIPS due to the equilibrium between $F_{wet\text{-}grad}$ and $F_{B//}$ (**Figure 5**a and Movie S5, Supporting Information). Accordingly, the experimental
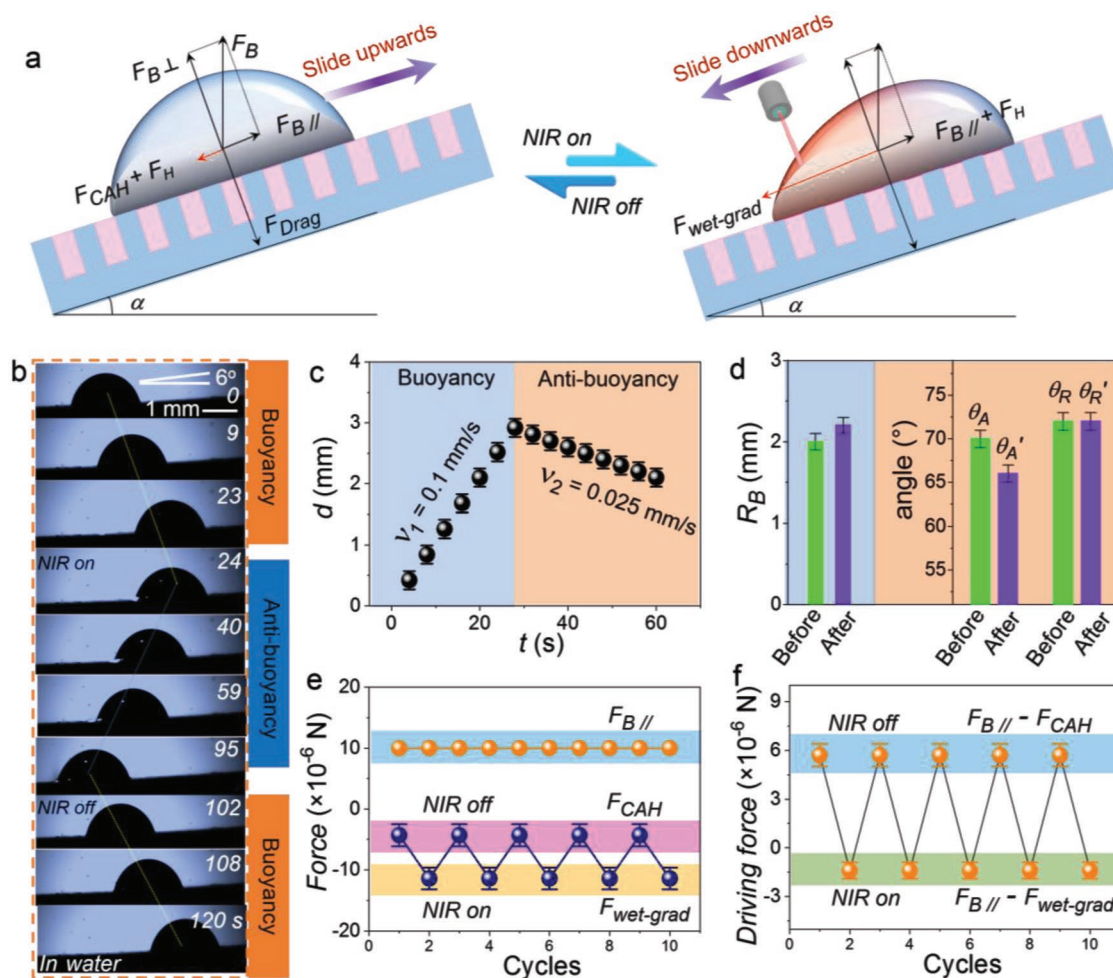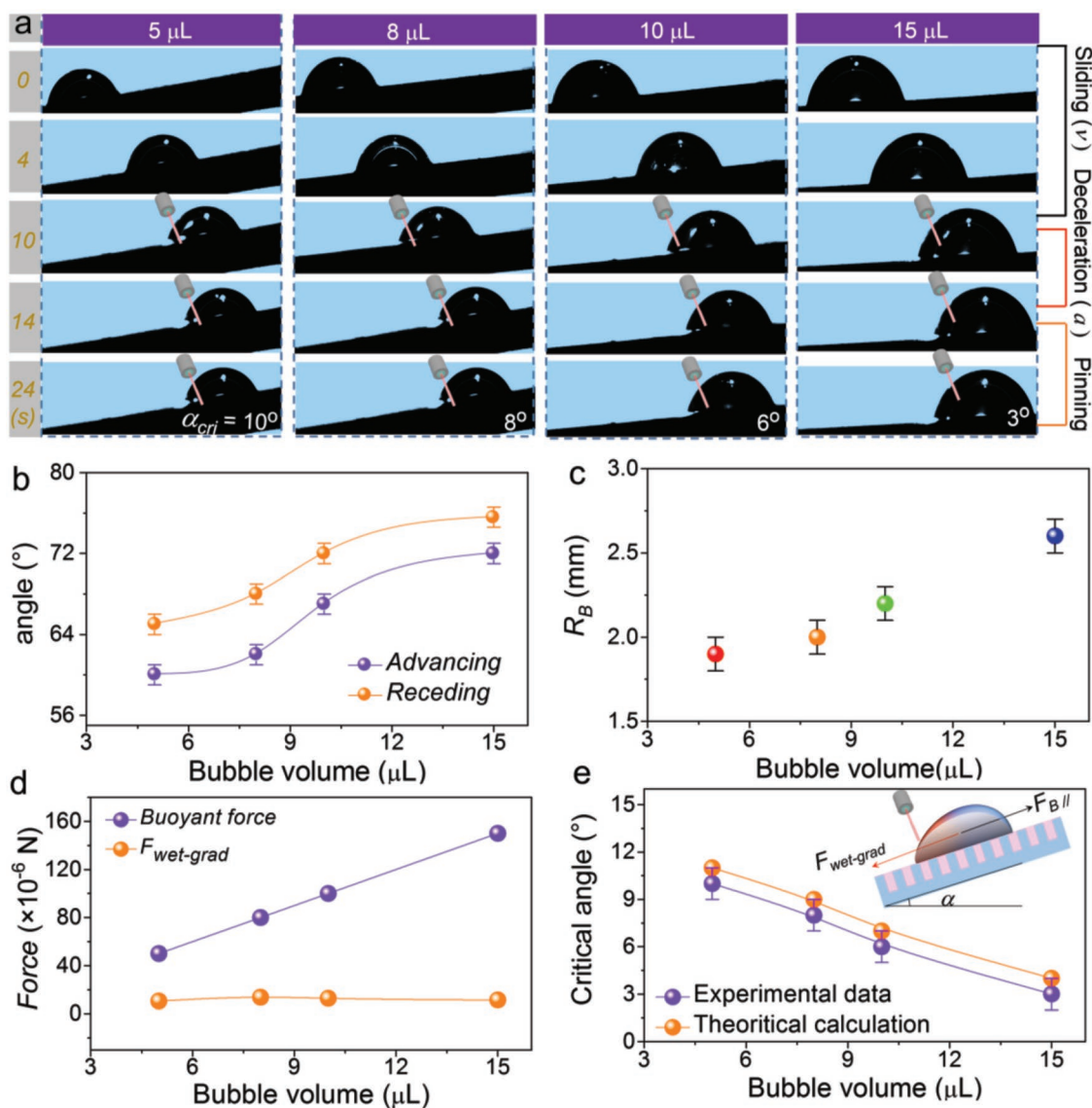
**Figure 4.** Antibuoyancy steering of UGB on inclined SLIPS. a) Force analysis for the UGB on an inclined SLIPS with and without NIR stimuli. b) The captured optical images of buoyancy-driven moving uphill and NIR-actuating (power density: $1.1 \times 10^2$ mW cm$^{-2}$, altitude: 8 cm) sliding downhill for UGB (10 µL) on an inclined SLIPS (lubricant: silicone oil, 10 mPa s; inclined angle: 6°). c) The recorded sliding distance $d$ as a function of time obtained from (a). d) The variations of $R_B$, $\theta_A$, and $\theta_B$ for UGB on the inclined SLIPS before and after loading NIR-stimuli. e) Theoretical calculation of $F_{B//}$ and experimental measurements of $F_{CAH}$ (NIR off) and $F_{wet-grad}$ (NIR on) for UGB on the inclined SLIPS and repetition stability test. f) The resultant force variation during the buoyancy-driven moving uphill and NIR-actuating sliding downhill processes. By loading/discharging NIR-stimuli, the driving force could be repeatedly switched between $-1.4$ and $5.7$ ($\times 10^{-6}$) N with ease.

$\alpha_{cri}$ for UGBs with the volume of 5, 8, 10, and 15 µL were measured as 10°, 8°, 6°, and 3°, respectively. In addition, their corresponding $\theta_A/\theta_R$ were characterized as 60/65°, 62/68°, 67/72°, 72/75° (Figure 5b), respectively. The measured $R_B$ for a series of UGBs on smart SLIPS with different $\alpha_{cri}$ were detected as 1.4, 1.9, 2.0, 2.2, and 2.6 mm (Figure 5c), respectively. According to Equation (1), $F_{CAH}$ for UGBs with the volume of 5, 8, 10, and 15 µL on smart SLIPS were successively calculated as 10.53, 13.68, 12.83, and 11.42 ($\times 10^{-6}$) N (Figure 5d). The buoyant forces for UGBs was proportional to the bubble volume and their numerical values were obtained as 50, 80, 100, and 150 ($\times 10^{-6}$) N, respectively. According to Equation (4), the theoretical $\alpha_{cri}$ values were calculated as 11°, 9°, 7°, and 4° that agree well with the experimental results (Figure 5e). Above investigations are expected to provide a significant guidance for antibuoyancy steering of UGBs by NIR actuation on smart SLIPS.

## 2.5. Programmable Horizontal Manipulation for UGBs on Planar SLIPS

In comparison with traditional Nepenthes-inspired slippery surfaces, the functional planar SLIPS cooperating with NIR-trigger explored in this work presents more versatile performances such as on-demand manipulating UGBs to desirable positions, accelerating UGB coalesced efficiency and achieving the dynamic control for UGB between sliding and pinning, in addition to realizing the UGB unidirectional transport. As shown in **Figure 6**a–d, the freestanding UGBs on planar SLIPS could be horizontally steered to a "USTC" pattern as we desired by a tracing NIR-stimuli. Thereafter, these patterned UGBs could be in succession merged into a bigger UGB by virtue of the same mechanism. Furthermore, the dynamic control between the sliding and pinning states of UGB can be introduced to optical systems for light regulation, facilitating a facile light-control-light

**ADVANCED**
**SCIENCE NEWS**
www.advancedsciencenews.com

**ADVANCED**
**FUNCTIONAL**
**MATERIALS**
www.afm-journal.de

**Figure 5.** Critical-angle exploration for antibuoyancy steering diverse UGBs. a) The captured optical images presenting the i) buoyancy-driven moving uphill (0–10 s, uniform motion, $v$), ii) NIR-actuating (power density: $1.1 \times 10^2$ mW cm$^{-2}$, altitude: 8 cm) deceleration (10–14 s, negative acceleration, $-a$), and iii) pinning still due to the equilibrium between $F_{B//}$ and $F_{wet\text{-}grad}$ for UGBs (5, 8, 10, and 15 µL) on the inclined SLIPSs (lubricant: silicone oil, 10 mPa s; experimental critical-angles: 10°, 8°, 6°, and 3°). The measurements of b) $\theta_A$ and $\theta_B$ and c) $R_B$ for the UGBs pinning on the inclined SLIPSs obtained from (a). d) The calculated $F_B$ and $F_{wet\text{-}grad}$ for diverse UGBs pinning on the inclined SLIPSs. e) Comparison of critical-angles achieved from theoretical calculations and experimental measurements for diverse UGBs pinning on the inclined SLIPSs.

optical device. As the bubble can block the light at visible region, a remote optical shutter is realized on the smart SLIPS by taking advantage of loading/discharging a tracing NIR-stimuli (Figure 6e and Movie S6, Supporting Information). This optical demonstration unfolds new possibilities of SLIPS in wide applications including optofluidics and all-optical modulators.

## 3. Conclusion

In summary, a light-responsive SLIPS composed of selective lubricants and super-hydrophobic PAF ablated by one-step femtosecond laser vertically crossed scan has been successfully

fabricated. Relying on this planar SLIPS, we can horizontally actuate gas bubbles at arbitrary directions by simply loading/discharging unilateral NIR-stimuli. The underlying mechanism is that a giant wettability gradient force ($F_{wet\text{-}grad}$) originated from temperature difference would generate within 1 s in the presence of unilateral NIR-trigger due to the photothermal effect of $Fe_3O_4$ NPs embedded in smart SLIPS. Once the NIR-stimuli are discharged, the instantaneous vanish of temperature difference and $F_{wet\text{-}grad}$ would immediately decelerate the UGB on smart SLIPS from sliding to pinning. On this basis, we quantitatively study the relationship among and bubble volume/lubricant rheological parameters, $F_{wet\text{-}grad}$ and sliding velocity. The smaller the bubble volume, the larger the bubble
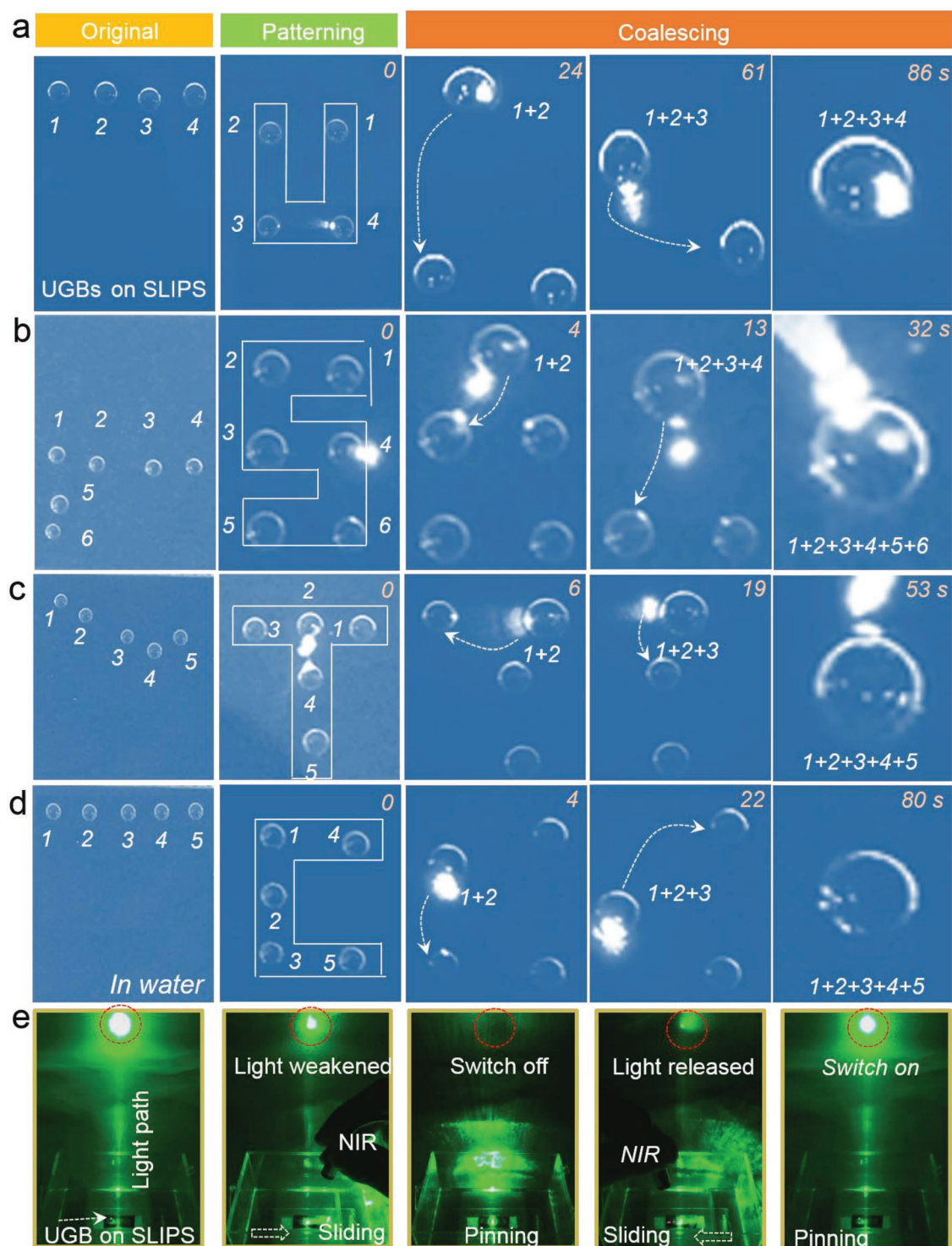
**Figure 6.** Programmable manipulation for UGBs on horizontal planar SLIPS. a–d) Digital pictures of steering UGBs on-demand to form a desired pattern "USTC" by controllable NIR-stimuli and subsequently merge into a bigger gas bubble. e) Demonstration of a facile remote light-control-light shutter enabled by loading and discharging NIR-stimuli on planar SLIPS.

sliding velocity. The lower the lubricant viscosity, the larger the bubble sliding velocity. Furthermore, the fundamental physics renders us the achievement of antibuoyancy manipulating the UGBs by taking advantage of inclined SLIPS and NIR-stimuli.

By combining the experimental measurements and theoretical calculations, we also harvest the key $\alpha_{cri}$ for UGBs with disparate volumes on inclined SLIPSs. Significantly, by virtue of the controllable $F_{wet\text{-}grad}$, we can steer the NIR-actuating UGBs

**ADVANCED**
**SCIENCE NEWS**
www.advancedsciencenews.com

**ADVANCED**
**FUNCTIONAL**
**MATERIALS**
www.afm-journal.de

to configurate a targeted pattern and regulate optical shutter. Compared with previous Nepenthes-inspired slippery surfaces, this light-responsive SLIPS independent of geography/buoyancy is more functional and precise at controlling various UGB's sliding speed, direction, and tracks. This work provides an innovative insight for designing smart slippery surfaces to achieve the controllable manipulation of gas bubbles in aqueous mediums.

## 4. Experimental Section

*Materials*: $Fe_3O_4$ NPs (diameter: 10 nm) were obtained from Tianjin kaili metallurgical research institute. PDMS silicone elastomer obtained from Dow Corning (Sylgard 184) was used as the host matrix. PDMS is a two-part solvent-free flexible silicone organic polymer in the form of a base compound with a separate hydrosilane curing agent that acts as a crosslinker. FC3283 were provided by Shengzheng Sino-Fluorine Technology Co., Ltd. Silicone oil (10 mPa s) was purchased from Dow Corning. Liquid paraffin was donated by Guangzhou Changrong Chemical Co. Ltd. Castor oil was provided by Jining Tianfu Oil Co. Ltd. Hexadecane was purchased from Sinopharm Chemical Reagent Co., Ltd. Distilled water ($H_2O$, 1 g cm$^{-3}$ density) served as contact angle test materials.

*Preparation of Smart SLIPS*: $Fe_3O_4$ NPs and PDMS prepolymer were mechanically mixed for 10 min at 1000 rpm. Thereafter, PDMS curing agent was added (10:1 ratio of the base and curing agent) and blended into the mixture by stirring manually before mechanical mixing again for 10 min at 1000 rpm. The prepared mixture composed of nanofillers and PDMS were poured into the home-made mold, and then placed in a vacuum chamber for 20 min for the removal of air bubbles and followed by curing at 80 °C for 2 h. The cured $Fe_3O_4$ NPs/PDMS composites were carefully peeled off from the mold and then ablated by programmable femtosecond laser. Typically, the super-hydrophobic PAF was manufactured by vertically crossed scanning of femtosecond laser. The laser beam (104 fs, 1 kHz, 800 nm) from a regenerative amplified Ti:sapphire femtosecond laser system (Legend Elite-1K-HE, Coherent, USA) was employed for ablation. During the fabrication process, the laser beam was guided onto the sample via a galvanometric system (SCANLAB, Germany), which made the laser beam focus and scan along the x/y coordinate direction. The laser power, scan spacing, and speed were set at 250 mW, 100 μm, and 4 mm s$^{-1}$, respectively. SLIPS samples were prepared by immersing the as-prepared PAF in various lubricant species for 24 h before analysis. PDMS became expanded and infused because the polymer chains extend to maximize polymer solvent interactions.[24] The excess lubricant on SLIPS was removed by standing the samples vertically for 10 min. Finally, SLIPS was successfully fabricated.

*Manipulation of UGBs on Smart SLIPS*: The NIR laser (FU808AD300-BC/BD10, Fuzhe Technology Co., Ltd., China) with wavelength of 808 nm (300 mW; spot area, 1.4 × 2.3 mm) was used for UGB manipulation on SLIPS. The size (width × length) of the NIR laser generator was 10 × 30 mm. The irradiation distance of NIR was adjusted in the range of 10–50 cm by a home-made holder. In this work, the irradiation distance of NIR was fixed as 8 cm. UGBs were steered by following the movement of NIR laser spot in desired routes.

*Characterization*: The micro/nanostructure induced by the laser was characterized by using a field-emission scanning electron microscope (SEM, JSM-6700F, Japan). The contact angles of the water droplet (≈5 μL) in air were measured using a CA100C contact-angle system (Innuo, China) with the sessile drop method. The average values were obtained by measuring five drops at different locations on the same surface. All the contact angle measurements were conducted at 10% humidity and 20 °C temperature. The surface temperature of NIR irradiating on SLIPS was measured by a thermal infrared camera (VarioCAMhr head 680, InfraTec).

## Supporting Information

Supporting Information is available from the Wiley Online Library or from the author.

## Conflict of Interest

The authors declare no conflict of interest.

[1] H. Ødegaard, *Water Sci. Technol.* **2001**, *43*, 75.
[2] M. S. K. A. Sarkar, S. W. Donne, G. M. Evans, *Adv. Powder Technol.* **2010**, *21*, 412.
[3] D. W. Fuerstenau, R. Herrera-Urbina, *Surfactant Sci. Ser.* **1989**, *33*, 259.
[4] M. J. F. Warnier, M. De Croon, E. V. Rebrov, J. C. Schouten, *Microfluid. Nanofluid.* **2010**, *8*, 33.
[5] C. A. Fairfield, *Wear* **2014**, *317*, 92.
[6] A. Philipp, W. Lauterborn, *J. Fluid Mech.* **1998**, *361*, 75.
[7] S. Fontanesi, M. Giacopini, G. Cicalese, S. Sissa, S. Fantoni, *Eng. Failure Anal.* **2014**, *44*, 408.
[8] C. Reynolds, M. Yitayew, *Agric. Water Manage.* **1995**, *29*, 25.
[9] Z. Y. Lu, W. Zhu, X. Y. Yu, H. C. Zhang, Y. J. Li, X. M. Sun, X. W. Wang, H. Wang, J. M. Wang, J. Luo, X. D. Lei, L. Jiang, *Adv. Mater.* **2014**, *26*, 2683.
[10] Y. J. Li, H. C. Zhang, T. H. Xu, Z. Y. Lu, X. C. Wu, P. B. Wan, X. M. Sun, L. Jiang, *Adv. Funct. Mater.* **2015**, *25*, 1737.
[11] V. Camel, A. Bermond, *Water Res.* **1998**, *32*, 3208.
[12] H. C. Yang, J. Hou, L. Wan, V. Chen, Z. K. Xu, *Adv. Mater. Interfaces* **2016**, *3*, 1500774.
[13] D. Lohse, X. H. Zhang, *Rev. Mod. Phys.* **2015**, *87*, 981.
[14] C. G. L. Furmidge, *J. Colloid Sci.* **1962**, *17*, 309.
[15] C. M. Yu, M. Y. Cao, Z. C. Dong, J. M. Wang, K. Li, L. Jiang, *Adv. Funct. Mater.* **2016**, *26*, 3236.
[16] C. M. Yu, X. B. Zhu, M. Y. Cao, C. L. Yu, K. Li, L. Jiang, *J. Mater. Chem. A* **2016**, *4*, 16865.
[17] C. H. Zhang, B. Zhang, H. Y. Ma, Z. Li, X. Xiao, Y. H. Zhang, X. Y. Cui, C. M. Yu, M. Y. Cao, L. Jiang, *ACS Nano* **2018**, *12*, 2048.
[18] C. H. Zhang, M. Y. Cao, H. Y. Ma, C. L. Yu, K. Li, C. M. Yu, L. Jiang, *Adv. Funct. Mater.* **2017**, *27*, 1702020.

[19] C. M. Yu, X. B. Zhu, K. Li, M. Y. Cao, L. Jiang, *Adv. Funct. Mater.* **2017**, *27*, 1701605.

[20] Y. L. Jiao, X. D. Lv, Y. Y. Zhang, C. Z. Li, J. W. Li, H. Wu, Y. Xiao, S. Z. Wu, Y. L. Hu, D. Wu, J. R. Chu, *Nanoscale* **2019**, *11*, 1370.

[21] P. Guo, Z. B. Wang, L. P. Heng, Y. Q. Zhang, X. Wang, L. Jiang, *Adv. Funct. Mater.* **2019**, *29*, 1808717.

[22] M. D. Shirk, P. A. Molian, *J. Laser Appl.* **1998**, *10*, 18.

[23] C. Gao, L. Wang, Y. Lin, J. Li, Y. Liu, X. Li, S. Feng, Y. M. Zheng, *Adv. Funct. Mater.* **2018**, *28*, 1803072.

[24] J. D. Smith, R. Dhiman, S. Anand, E. Reza-Garduno, R. E. Cohen, G. H. McKinley, K. K. Varanasi, *Soft Matter* **2013**, *9*, 1772.

[25] N. Bjelobrk, H. L. Girard, S. B. Subramanyam, H. M. Kwon, D. Quéré, K. K. Varanasi, *Phys. Rev. Fluids* **2016**, *1*, 063902.

**1904766 (11 of 11)**